

A Quantum Walk Inspired Qubit Lattice Algorithm for Simulating Electromagnetic Wave Propagation and Scattering in Conservative and Dissipative Magnetized Plasmas

Efstratios Koukoutsis,^{1,*} Kyriakos Hizanidis,¹ George Vahala,²
Christos Tsironis,¹ Abhay K. Ram,³ Min Soe,⁴ and Linda Vahala⁵

¹*School of Electrical and Computer Engineering,
National Technical University of Athens, Zographou 15780, Greece*

²*Department of Physics, William & Mary, Williamsburg, Virginia 23187, USA*

³*Plasma Science and Fusion Center, Massachusetts Institute of Technology, Cambridge, Massachusetts 02139, USA*

⁴*Department of Mathematics and Physical Sciences,
Rogers State University, Claremore, Oklahoma 74017, USA*

⁵*Department of Electrical and Computer Engineering,
Old Dominion University, Norfolk, Virginia 23529, USA*

(Dated: April 1, 2025)

Based on the Dirac representation of Maxwell equations we present an explicit, discrete space-time, quantum walk-inspired algorithm suitable for simulating the electromagnetic wave propagation and scattering from inhomogeneities within magnetized plasmas. The quantum walk is implemented on a lattice with an internal space of $n_q = 4$ -qubits, used to encode the classical field amplitudes. Unitary rotation gates operate within this internal space to generate the non-trivial dynamics of the free plasma-Dirac equation. To incorporate the contributions from the cyclotron and plasma density terms—manifesting as inhomogeneous potential terms—in the plasma-Dirac equation, the walk process is complemented with unitary potential operators. This leads to a unitary qubit lattice sequence that recovers the plasma-Dirac equation under a second-order accurate discretization scheme. The proposed algorithm is explicit and demonstrates, in the worst case, a polynomial quantum advantage compared to the Finite Difference Time Domain (FDTD) classical method in terms of resource requirements and error complexity. In addition, we extend the algorithm to include dissipative effects by introducing a phenomenological collision frequency between plasma species. Then, a post-selective time-marching implementation scheme is delineated, featuring a non-vanishing overall success probability and, subsequently, eliminating the need for amplitude amplification of the output state while preserving the quantum advantage.

I. INTRODUCTION

Quantum walks (QW) being the quantum counterparts of classical random walks [1, 2] play important role in quantum computing and particularly in quantum simulation [3–6]. Also, they have been established as universal model of quantum computation [7]. In particular, discrete-time quantum walks (DTQW) on regular lattices can give rise to wave equations for relativistic particles in the continuum limit [8–10] enabling an efficient simulation process. In the standard notation of DTQW, the dynamics of a particle are described by a walking exterior space \mathcal{H}_S and an interior 2-dimensional Hilbert space \mathcal{H}_C dubbed as the coin/spin space in which different unitary coin operators \hat{C} generating various non-trivial dynamics. The walking process is applied between the vertexes of the lattice though the streaming unitary operator \hat{S} acting on the $\{|p\rangle\} \in \mathcal{H}_S$ register in respect of the spin register,

$$\hat{S} = |0\rangle\langle 0| \otimes |p+1\rangle\langle p+1| + |1\rangle\langle 1| \otimes |p-1\rangle\langle p|. \quad (1)$$

Thus, the evolution of the state $|\psi(t)\rangle \in \mathcal{H} = \mathcal{H}_C \otimes \mathcal{H}_S$,

$$|\psi(t)\rangle = \sum_{p=0}^{2^n-1} (\psi_0(t)|0\rangle + \psi_1(t)|1\rangle) \otimes |p\rangle \quad (2)$$

from time t to $t + \Delta t$ is

$$|\psi(t + \Delta t)\rangle = \hat{S}(\hat{C} \otimes \hat{I})|\psi(t)\rangle. \quad (3)$$

For a general 3-dimensional collocated lattice, (resulting from the discretization of the configuration space $\mathcal{V} = [j_0, j_0 + L_j]^3 \subset \mathbb{R}^3$, comprised of N_j nodes separated by $\delta_j = L_j/N_j$ for each axis $j = x, y, z$), the $|p\rangle$ state describes the position of the particle in each lattice node,

$$|p\rangle = \bigotimes_j |p_j\rangle, \quad |p_j\rangle = |j_0 + p_j \delta_j\rangle, \quad n_p = \sum_j \log_2 N_j. \quad (4)$$

In Eq.(4), n_p is the number of qubits characterizing the $|p\rangle$ state. In contrast with random walks the evolution in Eq.(3) is unitary, hence reversible.

On increasing the dimension of the spin space \mathcal{H}_C into d -dimensions, we can extend QW algorithms to multi-dimensional and multi-particle quantum secular automata [11–13], quantum lattice Boltzmann [14] and, eventually, qubit lattice algorithms (QLA) [15, 16]. In

* stkoukoutsis@mail.ntua.gr

particular, QLA's backbone for the quantum representation of Maxwell equations in a general passive electromagnetic medium is based on the massless Dirac-type equation. This has then permitted quantum extensions to handle Maxwell equations in complex media [17–22]. The advantage of the aforementioned QW-inspired algorithms lie on the fact that the walking process can be implemented efficiently in the lattice as it will be showcased later.

Classical Maxwell equations have recently emerged as a compelling set of differential equations for applying quantum algorithms [23–29], primarily due to their (i) inherent linearity within the linear response framework and (ii) broad applicability to various physical problems. Albeit the significant contributions of the previous studies, most have focused on simplified models of wave propagation and scattering in either homogeneous or inhomogeneous scalar media. In addition the quantum implementation is based on unitary oracle operations, prohibiting an explicit implementation on quantum hardware. Such limitations mitigate the impact and the capabilities that these algorithms can have in realistic applications where the electromagnetic media response is anisotropic, inhomogeneous and potentially complex meaning that it can be dispersion and dissipation in the medium's response.

To this direction, based on the quantum representation of Maxwell equations in a cold magnetized plasma [21], by exploiting the Pauli structure of the generator of dynamics we present an explicit qubit lattice algorithm quantum encoded as a DTQW for simulation of electromagnetic wave propagation and scattering in inhomogeneous magnetized plasmas. The algorithm is explicit in terms of the required quantum resources and gate scaling as well as it exhibits a potential exponential quantum advantage compared to the contemporary and widely used Finite Difference Time Domain (FDTD) computational method [30, 31] for studying electromagnetic wave scattering in plasmas [32, 33].

The paper is organized as follows. Section II A outlines the theoretical reformulation of Maxwell equations for a cold magnetized plasma as a quantum Dirac equation. In Sec. II B, the details of encoding and discretization of the continuous plasma-Dirac system into qubit states are presented. Section III covers the algorithmic process, its explicit quantum circuit implementation, and the complexity scaling, demonstrating a quantum advantage over the FDTD method. Section IV A introduces a phenomenological collisional dissipation process that breaks the unitary evolution of the conservative case. Then, Sec. IV B presents a post-selective quantum algorithm based on the LCU method with an optimal overall success implementation probability. As a result, the previously established quantum advantage is maintained.

II. QUANTUM REPRESENTATION AND ENCODING

In this section we briefly revisit the theoretical construction of Maxwell equations in a cold magnetized plasma as a multi-spinor massless Dirac equation with a potential and expresses the electromagnetic state vector as a quantum state $|\psi\rangle \in \mathcal{H} = \mathcal{H}_C \otimes \mathcal{H}_S$.

A. Dirac representation of Maxwell equations in cold magnetized plasmas

Cold magnetized plasmas are gyrotropic i.e. anisotropic dielectric media exhibiting temporal dispersion with a frequency dependent permittivity matrix $\tilde{\epsilon}(\omega)$ in the frequency domain. Following the Stix notation [34],

$$\tilde{\epsilon}(\omega) = \begin{bmatrix} S & -iD & 0 \\ iD & S & 0 \\ 0 & 0 & P \end{bmatrix} \quad (5)$$

with

$$\begin{aligned} S &= \epsilon_0 \left(1 - \sum_{j=i,e} \frac{\omega_{pj}^2}{\omega^2 - \omega_{cj}^2} \right) \\ D &= \epsilon_0 \sum_{j=i,e} \frac{\omega_{cj} \omega_{pj}^2}{\omega(\omega^2 - \omega_{cj}^2)} \\ P &= \epsilon_0 \left(1 - \sum_{j=i,e} \frac{\omega_{pj}^2}{\omega^2} \right). \end{aligned} \quad (6)$$

The definition of the elements in Eq.(6) in the Stix permittivity tensor is taken for a two-species, ions (i) and electrons (e), plasma with inhomogeneous plasma frequency $\omega_{pj}^2(\mathbf{r}) = \frac{n_j(\mathbf{r})q_j^2}{m_j\epsilon_0}$ where $n_j(\mathbf{r})$ is the j^{th} species number density. The cyclotron frequency $\omega_{cj} = \frac{q_j B_0}{m_j}$ is defined in respect of a homogeneous magnetic field B_0 along the z axis and m_j, q_j are the mass and charge of the j -species respectively.

In the temporal domain, the source free Maxwell equations in terms of the electromagnetic intensity $\mathbf{d} = (\mathbf{D}, \mathbf{B})^T$ and electromagnetic fields $\mathbf{u} = (\mathbf{E}, \mathbf{H})^T$ are compactly written as,

$$i \frac{\partial \mathbf{d}}{\partial t} = \hat{M} \mathbf{u}, \quad \nabla \cdot \mathbf{d} = 0. \quad (7)$$

The \hat{M} operator in Eq.(7),

$$\hat{M} = i \begin{bmatrix} 0_{3 \times 3} & \nabla \times \\ -\nabla \times & 0_{3 \times 3} \end{bmatrix} \quad (8)$$

is a self adjoint operator $\hat{M} = \hat{M}^\dagger$ in the domain $\mathcal{D}(\hat{M}) = L^2(\mathcal{V} \subset \mathbb{R}^3, \mathbb{C}^6)$ under the boundary condition $\mathbf{n}(\mathbf{r}) \times \mathbf{E} = 0$ with $\mathbf{n}(\mathbf{r})$ being the outward orthogonal vector

in the boundary $\partial\mathcal{V}$. The divergence set of equations in Eq.(7) are treated as initial conditions.

Given the fact that the permittivity tensor $\tilde{\epsilon}(\omega)$ is Hermitian there is conservation of a positive definite energy which is a suffice condition for the dynamics to be recast in an explicit quantum representation with Hermitian structure [35]. As a result, following [21], transforming into the temporal domain we obtain an augmented version of Maxwell equations in a form of a massless and multi-spinor Dirac equation with a potential $\hat{V}(\mathbf{r})$,

$$i\frac{\partial\psi}{\partial t} = \left[-c\hat{P}_{E,B} \otimes \hat{\gamma}_{em} \cdot \hat{\mathbf{p}} + \hat{V}(\mathbf{r}) \right] \psi. \quad (9)$$

The ψ state in the plasma Dirac equation (9) contain the pertinent electromagnetic fields and current densities,

$$\psi = \begin{bmatrix} \epsilon_0^{1/2} \mathbf{E} \\ \mu_0^{1/2} \mathbf{H} \\ \frac{1}{\epsilon_0^{1/2} \omega_{pi}} \mathbf{J}_{ci} \\ \frac{1}{\epsilon_0^{1/2} \omega_{pe}} \mathbf{J}_{ce} \end{bmatrix}, \quad \mathbf{J}_{cj} = \int_0^t \frac{\partial \hat{K}_j(t-\tau)}{\partial t} \mathbf{E}(\mathbf{r}, \tau) d\tau, \quad (10)$$

where $\hat{K}_j(t)$ is the susceptibility kernel contribution for each species in the temporal domain,

$$\hat{K}(t) = \epsilon_0 \sum_{j=i,e} \begin{bmatrix} \frac{\omega_{pj}^2}{\omega_{cj}} \sin \omega_{cj} t & \frac{\omega_{pj}^2}{\omega_{cj}} (\cos \omega_{cj} t - 1) & 0 \\ \frac{\omega_{pj}^2}{\omega_{cj}} (1 - \cos \omega_{cj} t) & \frac{\omega_{pj}^2}{\omega_{cj}} \sin \omega_{cj} t & 0 \\ 0 & 0 & \omega_{pj}^2 t \end{bmatrix} \\ = \hat{K}_i(t) + \hat{K}_e(t). \quad (11)$$

The electromagnetic Dirac matrices $\hat{\gamma}_{el} = (\hat{\gamma}_x, \hat{\gamma}_y, \hat{\gamma}_z)$ read,

$$\hat{\gamma}_i = \hat{\sigma}_y \otimes \hat{S}_i, \quad i = x, y, z, \quad (12)$$

where $\hat{\sigma}_y$ is the Pauli y -matrix and \hat{S}_i are the spin-1 matrices,

$$\hat{S}_x = \begin{bmatrix} 0 & 0 & 0 \\ 0 & 0 & -i \\ 0 & i & 0 \end{bmatrix}, \quad \hat{S}_y = \begin{bmatrix} 0 & 0 & i \\ 0 & 0 & 0 \\ -i & 0 & 0 \end{bmatrix}, \quad \hat{S}_z = \begin{bmatrix} 0 & -i & 0 \\ i & 0 & 0 \\ 0 & 0 & 0 \end{bmatrix}. \quad (13)$$

Finally, $c = (\epsilon_0 \mu_0)^{-1/2}$ is the speed of light in the vacuum, $\hat{\mathbf{p}} = -i\nabla$ is the the quantum mechanical momentum operator, $\hat{P}_{E,H} = (\sigma_z + I_{2 \times 2})/2$ is the projection operator in the subspace of the electromagnetic fields $\{\mathbf{E}, \mathbf{H}\}$ and the Hermitian potential operator $\hat{V}(\mathbf{r})$ is [21],

$$\hat{V}(\mathbf{r}) = \begin{bmatrix} 0_{3 \times 3} & 0_{3 \times 3} & -i\omega_{pi} & -i\omega_{pe} \\ 0_{3 \times 3} & 0_{3 \times 3} & 0_{3 \times 3} & 0_{3 \times 3} \\ i\omega_{pi} & 0_{3 \times 3} & \omega_{ci} \hat{S}_z & 0_{3 \times 3} \\ i\omega_{pe} & 0_{3 \times 3} & 0_{3 \times 3} & \omega_{ce} \hat{S}_z \end{bmatrix}. \quad (14)$$

The positive definite conserved electromagnetic energy

$E(t)$ reads,

$$E(t) = \int_{\mathcal{V}} \left(\epsilon_0 |\mathbf{E}|^2 + \frac{|\mathbf{B}|^2}{\mu_0} \right) d\mathbf{r} + \\ + \int_{\mathcal{V}} \left(\frac{|\mathbf{J}_{ci}|^2}{\epsilon_0 \omega_{pi}^2(\mathbf{r})} + \frac{|\mathbf{J}_{ce}|^2}{\epsilon_0 \omega_{pe}^2(\mathbf{r})} \right) d\mathbf{r}, \quad \mathcal{V} \subset \mathbb{R}^3. \quad (15)$$

The first integrand terms on the right hand side in Eq.(15) correspond to the electromagnetic field energy density, while the next two integrand terms are the kinetic energy density associated with the electrons and ions in the plasma [36].

B. Discretization and encoding

For simplicity we will assume a $x - y$ uniform lattice with discretization step $\delta_x = \delta_y = \delta$ so for the configuration space $\mathcal{V} = [x_0, x_0 + L_x] \times [y_0, y_0 + L_y]$ to be comprised of $N_x N_y$ nodes separated by δ in each x, y axes. As a result, in analogous way with Eq.(2), the classical plasma state ψ in Eq.(10) can be written as a $n_p = \log_2(N_x N_y) = n_{px} + n_{py}$ qubits pure state,

$$\psi(\mathbf{r}, t) \rightarrow |\psi(t)\rangle = \sum_{p=0}^{2^{n_p}-1} |\psi_q(t)\rangle \otimes |p\rangle \in \mathcal{H} = \mathcal{H}_C \otimes \mathcal{H}_S, \quad (16)$$

where the state $|\psi_q\rangle \in \mathcal{H}_C$ depends on the dimensionality of the plasma state ψ and it will be discussed later.

By defining the state $|\psi_p(t)\rangle = |\psi_q(t)\rangle \otimes |p\rangle$ we can express the momentum operator in the plasma Dirac equation in the discretized lattice space in each dimension using a Euler difference scheme. For example in the in the x direction for the forward difference,

$$\frac{|\psi_p(t + \Delta t)\rangle - |\psi_p(t)\rangle}{\Delta t} + O(\Delta t) = \frac{c}{\Delta x} \left(|\psi_{p+1}(t)\rangle - |\psi_p(t)\rangle \right) + O(\Delta x). \quad (17)$$

Then, to first order accuracy $\Delta x \sim \delta$, $\Delta t = \Delta x/c \sim \delta$, Eq.(17) reads,

$$|\psi_p(t + \Delta t)\rangle = \hat{S} |\psi_p(t)\rangle + O(\delta^2). \quad (18)$$

The \hat{S} operator in Eq.(18) is the streaming operator $\hat{S}|p\rangle = |p+1\rangle$. Therefore, the temporal evolution in Eq.(18), in the continuous limit $\delta \rightarrow 0$ recovers to first order

$$i\frac{\partial\psi(x, t)}{\partial t} = -c\hat{p}_x \psi(x, t) + O(\delta). \quad (19)$$

Applying forward \hat{S} and backward \hat{S}^\dagger steaming operations as well as alternating \hat{C} and \hat{C}^\dagger operations between different lattice sites we aiming into a discretization scheme under which the continuous evolution is recovered to second order $O(\delta^2)$, compared to Eq.(19), to

ensure stability. The produced sequence is a QLA sequence that extends the DTQW evolution in Eq.(3).

The advantage of using the streaming operation in a quantum computer lies on its recursive structure [37] that allows for efficient implementation within $O(n_p^2)$ elementary gates. Specifically, expressing $|p\rangle$ in its binary form $|p_{n_p-1}p_{n_p-2}\dots p_0\rangle$, the quantum respective circuit implementation of the unitary \hat{S} operator is depicted in Fig.1. Each of these n_p in numbers multi-controlled CNOTs act-

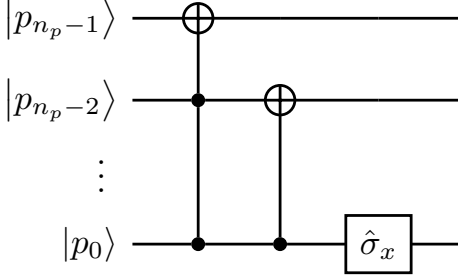


FIG. 1. Quantum gate implementation of streaming operator \hat{S} in the $|p\rangle$ register. The least significant bit is the p_0 . The recursive structure of the operation allows for a decomposition in $O(n_p^2)$ single-qubit and CNOT gates.

ing, at most, on n_p qubits can be decomposed in $O(n_p)$ elementary gates [38] and therefore the total implementations scales as $O(n_p^2)$.

What is left now is to encode the $|\psi_q\rangle$ state in the spin state to complement the walk process in the discretized lattice, allowing the action of coin operators to generate the evolution for Eq.(9). In contrast with the Dirac quantum 4-spinor the classical state ψ in Eq.(10) is 12-dimensional hence we need $n_q = 4$ qubits in general to encode the spinor components in the spin space $\mathcal{H}_C = \mathbb{C}^2 \otimes \mathbb{C}^2 \otimes \mathbb{C}^2 \otimes \mathbb{C}^2$. However, the question that arises is now how to encode the 12 classical amplitudes within the 16 basis elements of \mathcal{H}_C as pure state. We address this issue by considering the canonical form of a general 4-qubit pure state $|\psi\rangle_4$. In that way, the minimal number of local bases product states in terms of which the state $|\psi\rangle_4$ can be written is twelve [39],

$$\begin{aligned} |\psi\rangle_4 = & a|0000\rangle + b|0100\rangle + c|0101\rangle + d|0110\rangle \\ & + e|1000\rangle + f|1001\rangle + g|1010\rangle + h|1011\rangle \\ & + i|1100\rangle + j|1101\rangle + k|1110\rangle + l|1111\rangle. \end{aligned} \quad (20)$$

Therefore we assign the 12 states of the canonical 4-qubit generalized Schmidt decomposition (20) as the $\{|q\rangle\}$ register in respect of the components of the plasma state in

Eq.(10) as following:

$$\begin{aligned} \psi_0 &\leftrightarrow E_x \rightarrow |q_0\rangle \leftrightarrow |0000\rangle \\ \psi_1 &\leftrightarrow E_y \rightarrow |q_1\rangle \leftrightarrow |0100\rangle \\ \psi_2 &\leftrightarrow E_z \rightarrow |q_2\rangle \leftrightarrow |0101\rangle \\ \psi_3 &\leftrightarrow H_x \rightarrow |q_3\rangle \leftrightarrow |0110\rangle \\ \psi_4 &\leftrightarrow H_y \rightarrow |q_4\rangle \leftrightarrow |1000\rangle \\ \psi_5 &\leftrightarrow H_z \rightarrow |q_5\rangle \leftrightarrow |1001\rangle \\ \psi_6 &\leftrightarrow J_{cix} \rightarrow |q_6\rangle \leftrightarrow |1010\rangle \\ \psi_7 &\leftrightarrow J_{ciy} \rightarrow |q_7\rangle \leftrightarrow |1011\rangle \\ \psi_8 &\leftrightarrow J_{ciz} \rightarrow |q_8\rangle \leftrightarrow |1100\rangle \\ \psi_9 &\leftrightarrow J_{cey} \rightarrow |q_9\rangle \leftrightarrow |1101\rangle \\ \psi_{10} &\leftrightarrow J_{cey} \rightarrow |q_{10}\rangle \leftrightarrow |1110\rangle \\ \psi_{11} &\leftrightarrow J_{cez} \rightarrow |q_{11}\rangle \leftrightarrow |1111\rangle \end{aligned} \quad (21)$$

Therefore,

$$|\psi_q\rangle = \sum_{j=0}^{11} \psi_j |q_j\rangle, \quad (22)$$

and the total quantum encoded plasma state reads,

$$|\psi(t)\rangle = \sum_{j,p} \psi_{j,p}(t) |q_j\rangle \otimes |p\rangle \in \mathcal{H} = \mathcal{H}_C \otimes \mathcal{H}_S. \quad (23)$$

III. THE QUANTUM ALGORITHM

The plasma Dirac Eq.(9) is composed of a kinetic part $c\hat{\gamma}_{em} \cdot \hat{\mathbf{p}}$ corresponding to the electromagnetic propagation in the vacuum space which has been treated before in [15–17, 19, 20] using the inhomogeneous QW framework where the unitary coin operators \hat{C} depend on the discretization length δ [40]. In that way, we can retrieve the kinetic part to second order $O(\delta^2)$ under a diffusion scheme $\Delta t = D\Delta x^2 \sim \delta^2$ where $D = O(1)$ is a diffusion coefficient. This is in sheer contrast with the the simple first order scheme presented in Eqs.(17)-(19).

On the other hand, the potential term $\hat{V}(\mathbf{r})$ in the matrix form in Eq.(14) contributes only algebraically to Eq.(9) and no streaming will be incorporated. To retrieve those terms we will need to include some external operators beyond the quantum walk process.

A. The QLA sequence and the external operators

We aim for an evolution sequence $t \rightarrow t + \Delta t$ of the form,

$$|\psi(t + \Delta t)\rangle = \hat{V}_{pe} \hat{V}_{pi} \hat{V}_{ce} \hat{V}_{ci} \hat{U}_{QLA} |\psi(t)\rangle, \quad (24)$$

where \hat{U}_{QLA} is the unitary QLA sequence of streaming and coin operators related to the kinetic part whereas the \hat{V}_{cj} and \hat{V}_{pj} with $j = i, e$ are external unitary operators associated with the potential term $\hat{V}(\mathbf{r})$. Therefore,

using the full sequence in Eq.(24) we recover the plasma Dirac equation (9) to second order $O(\delta^2)$.

Fist we define the following coin operators, acting on each of the x, y directions in the 12-dimensional $|\psi_q\rangle \in \mathcal{H}_C$ spin state:

$$\hat{C}_X = \begin{bmatrix} \hat{C}_x & 0 \\ 0 & I_{6 \times 6} \end{bmatrix}, \quad (25)$$

with

$$\hat{C}_x = \begin{bmatrix} 1 & 0 & 0 & 0 & 0 & 0 \\ 0 & \cos \theta & 0 & 0 & 0 & -\sin \theta \\ 0 & 0 & \cos \theta & 0 & -\sin \theta & 0 \\ 0 & 0 & 0 & 1 & 0 & 0 \\ 0 & 0 & \sin \theta & 0 & \cos \theta & 0 \\ 0 & \sin \theta & 0 & 0 & 0 & \cos \theta \end{bmatrix}, \quad (26)$$

and

$$\hat{C}_Y = \begin{bmatrix} \hat{C}_y & 0 \\ 0 & I_{6 \times 6} \end{bmatrix}, \quad (27)$$

with

$$\hat{C}_y = \begin{bmatrix} \cos \theta & 0 & 0 & 0 & 0 & \sin \theta \\ 0 & 1 & 0 & 0 & 0 & 0 \\ 0 & 0 & \cos \theta & \sin \theta & 0 & 0 \\ 0 & 0 & -\sin \theta & \cos \theta & 0 & 0 \\ 0 & 0 & 0 & 0 & 1 & 0 \\ -\sin \theta & 0 & 0 & 0 & 0 & \cos \theta \end{bmatrix}, \quad (28)$$

where the rotation angle θ is $\theta \sim c\delta/4$. The non trivial part of coin operators \hat{C}_x and \hat{C}_y are two-level unitary rotations acting locally on the $|\mathbf{E}, \mathbf{H}\rangle$ subspace of the overall $|\psi_q\rangle$ state.

Then, the unitary QLA sequence for the kinetic part is $\hat{U}_{QLA} = \hat{U}_Y \hat{U}_X$, where \hat{U}_X, \hat{U}_Y are the respective sequence of unitary coin-streaming operators in each direction,

$$\hat{U}_X = \hat{S}_{25}^{+x} \hat{C}_X^\dagger \hat{S}_{25}^{-x} \hat{C}_X \hat{S}_{14}^{-x} \hat{C}_X^\dagger \hat{S}_{14}^{+x} \hat{C}_X \hat{S}_{25}^{-x} \hat{C}_X \hat{S}_{25}^{+x} \hat{C}_X^\dagger \hat{S}_{14}^{+x} \hat{C}_X \hat{S}_{14}^{-x} \hat{C}_X^\dagger, \quad (29)$$

$$\hat{U}_Y = \hat{S}_{25}^{+y} \hat{C}_Y^\dagger \hat{S}_{25}^{-y} \hat{C}_Y \hat{S}_{03}^{-y} \hat{C}_Y^\dagger \hat{S}_{03}^{+y} \hat{C}_Y \hat{S}_{25}^{-y} \hat{C}_Y \hat{S}_{25}^{+y} \hat{C}_Y^\dagger \hat{S}_{03}^{+y} \hat{C}_Y \hat{S}_{03}^{-y} \hat{C}_Y^\dagger. \quad (30)$$

In Eqs.(29) and (30) the streaming operator in each direction is defined similarly to Eq.(1) as

$$\hat{S}_{ij}^{+,x,y} = (|q_i\rangle \langle q_i| + |q_j\rangle \langle q_j|) \otimes \hat{S}^{+,x,y} + \sum_{k \in \{i,j\}} |q_k\rangle \langle q_k| \otimes I_{2^p \times 2^p}. \quad (31)$$

Since the streaming operator is unitary the walking process in the opposite direction is provided by $(\hat{S}_{ij}^{+,x,y})^\dagger = \hat{S}_{ij}^{-,x,y}$. The implementation of the streaming operator in the respective $|p_x\rangle$ and $|p_y\rangle$ registers follow that of Fig.1 and therefore scales as $O(n_{px}^2 + n_{py}^2)$.

To recover the algebraic contribution from the potential in Eq.(14) we decompose it into distinct contributions from the cyclotron and plasma frequency terms for each species, structured terms as follows,

$$\hat{V}(\mathbf{r}) = \hat{D}_{\omega_{pi}} + \hat{D}_{\omega_{pe}} + \hat{D}_{\omega_{ci}} + \hat{D}_{\omega_{ce}}, \quad (32)$$

with an underlying Pauli structure,

$$\hat{D}_{\omega_{pi}} = \frac{1}{2} \hat{\sigma}_y \otimes (I_{2 \times 2} + \hat{\sigma}_z) \otimes \omega_{pi}, \quad (33)$$

$$\hat{D}_{\omega_{pe}} = \frac{1}{2} (\hat{\sigma}_x \otimes \hat{\sigma}_y + \hat{\sigma}_y \otimes \hat{\sigma}_x) \otimes \omega_{pe}, \quad (34)$$

$$\hat{D}_{\omega_{ci}} = \frac{1}{4} (I_{2 \times 2} - \hat{\sigma}_z) \otimes (I_{2 \times 2} + \hat{\sigma}_z) \otimes \omega_{ci} \hat{S}_z, \quad (35)$$

$$D_{\omega_{ce}} = \frac{1}{4} (I_{2 \times 2} - \hat{\sigma}_z) \otimes (I_{2 \times 2} - \hat{\sigma}_z) \otimes \omega_{ce} \hat{S}_z. \quad (36)$$

The $\hat{\sigma}$ matrices in Eqs.(33)-(36) are the standard Pauli matrices.

As a result, to recover the non-differential terms associated with the plasma and magnetic inhomogeneity profiles, we have to define another set of unitary operators complementary to the QLA sequence. Specifically, for the diagonal cyclotron terms,

$$\hat{V}_{ci} = \begin{bmatrix} I_{6 \times 6} & 0_{6 \times 6} \\ 0_{6 \times 6} & \hat{v}_{ci} \end{bmatrix}, \quad \hat{V}_{ce} = \begin{bmatrix} I_{6 \times 6} & 0_{6 \times 6} \\ 0_{6 \times 6} & \hat{v}_{ce} \end{bmatrix}, \quad (37)$$

with

$$\hat{v}_{ci} = \begin{bmatrix} \cos \theta_{ci} & -\sin \theta_{ci} & 0 & 0 & 0 & 0 \\ \sin \theta_{ci} & \cos \theta_{ci} & 0 & 0 & 0 & 0 \\ 0 & 0 & 1 & 0 & 0 & 0 \\ 0 & 0 & 0 & 1 & 0 & 0 \\ 0 & 0 & 0 & 0 & 1 & 0 \\ 0 & 0 & 0 & 0 & 0 & 1 \end{bmatrix}, \quad \hat{v}_{ce} = \begin{bmatrix} 1 & 0 & 0 & 0 & 0 & 0 \\ 0 & 1 & 0 & 0 & 0 & 0 \\ 0 & 0 & 1 & 0 & 0 & 0 \\ 0 & 0 & 0 & \cos \theta_{ce} & -\sin \theta_{ce} & 0 \\ 0 & 0 & 0 & \sin \theta_{ce} & \cos \theta_{ce} & 0 \\ 0 & 0 & 0 & 0 & 0 & 1 \end{bmatrix}. \quad (38)$$

The rotation angles now read $\theta_{ci,e} \sim \delta^2 \omega_{ci,e}$. For simplicity we will assume homogeneous magnetic field so $\omega_{ci,e} = \text{constant}$. Similarly with the coin operators $\hat{C}_{X,Y}$ in Eqs.(25),(27) the cyclotron external potential operators are unitary rotation matrices acting on the locally in the spin register.

Moving on to the off-diagonal plasma inhomogeneity terms, we define $\hat{V}_{pi,e}$ as

$$\hat{V}_{pi} = \begin{bmatrix} \cos \theta_{pi} & 0 & -\sin \theta_{pi} & 0 \\ 0 & I_{3 \times 3} & 0 & 0 \\ \sin \theta_{pi} & 0 & \cos \theta_{pi} & 0 \\ 0 & 0 & 0 & I_{3 \times 3} \end{bmatrix}, \quad (39)$$

and

$$\hat{V}_{pe} = \begin{bmatrix} \cos \theta_{pe} & 0 & 0 & -\sin \theta_{pe} \\ 0 & I_{3 \times 3} & 0 & 0 \\ 0 & 0 & I_{3 \times 3} & 0 \\ \sin \theta_{pe} & 0 & 0 & \cos \theta_{pe} \end{bmatrix}. \quad (40)$$

The respective non-trivial elements in matrices (39) and (40) are diagonal 3×3 matrices with rotation angle $\theta_{pi} \sim \delta^2 \omega_{pi}$. By considering an inhomogeneous plasma profile $\omega_{pi,e} = \omega_{pi,e}(\mathbf{r})$ the external operators still possess a two-level rotational structure on the 4 qubit spin space \mathcal{H}_C but in contrast to the previous operators, their action changes in respect of the $\{|p\rangle\}$ register since the rotation angle θ_p depends on the value of the plasma density profile ω_p in the lattice site. Thus,

$$\hat{V}_p |\psi(t)\rangle = \sum_{j=0}^{11} \sum_{p=0}^{2^{n_p}-1} \psi_{j,p} \hat{\mathcal{R}}_y(2\theta_p(p)) |q_j\rangle \otimes |p\rangle, \quad (41)$$

with $\theta_p(p) \sim \delta^2 \omega_p(p)$. Take notice that in Eq.(41) the superscripts in θ_p and ω_p denote quantities related to plasma density and they are not summation indices. For the same reason, we have also suppressed indices i and e for the respective plasma species. The operator $\hat{\mathcal{R}}_y$ denotes a two-level \hat{R}_y rotation.

Finally, in the continuous limit $\delta \rightarrow 0$ the sequence in Eq.(24) recovers the Dirac representation of Maxwell system for the cold magnetized plasma (9) to order $O(\delta^2)$ under the diffusion ordering $\Delta t \sim \delta^2$. However, it must be highlighted that the sequence (24) has been produced through a perturbation expansion in terms of δ to recover the kinetic and potential terms (33)-(36) and not from Trotterization scheme i.e., separating the exponential evolution operator into a product of the exponential parts of kinetic and potential operators respectively. This is evident since the respective operators in the sequence (24) do not commute.

B. Quantum circuit implementation

In this section we provide explicit quantum circuit implementation of the participating operators in the evolution sequence Eq.(24) along with the respective gate cost, making the algorithm transparent and providing its implementation feasibility in actual hardware.

The QLA \hat{U}_{QLA} is comprised by the streaming operators whose implementation has been provided in Fig.1 and the coin operators which can be decomposed into two two-level \hat{R}_y rotations acting locally in the coin space \mathcal{H}_C . Hence, the implementation of their action in the assigned canonical basis of Eq.(21), is depicted in Figs.2 and 3, where

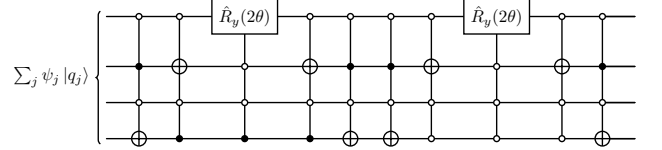


FIG. 2. Quantum circuit implementation of the \hat{C}_X operator in the $\{|q_j\rangle\}$ coin register. The spatial dependence has been suppressed for simplicity.

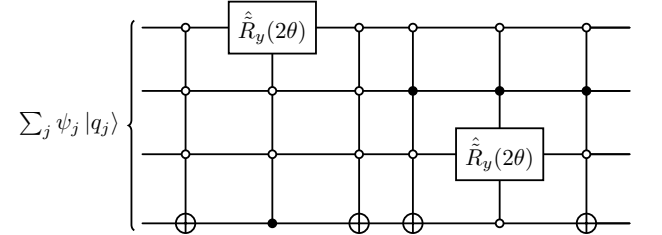


FIG. 3. Quantum circuit implementation of the \hat{C}_Y operator in the $\{|q_j\rangle\}$ coin register. The spatial dependence has been suppressed for simplicity.

$$\hat{R}_y(\theta) = \begin{bmatrix} \cos \frac{\theta}{2} & -\sin \frac{\theta}{2} \\ \sin \frac{\theta}{2} & \cos \frac{\theta}{2} \end{bmatrix} \quad \text{and} \quad \hat{\hat{R}}_y = \hat{\sigma}_z \hat{R}_y \hat{\sigma}_z. \quad (42)$$

Since each of the $\hat{C}_{X,Y}$ can be decomposed into two local two-level unitary operators acting on the 4-qubit register the implementations circuits in Figs.2 and 3 can be decomposed into $O(2 \cdot 4^2)$ single qubit and CNOT

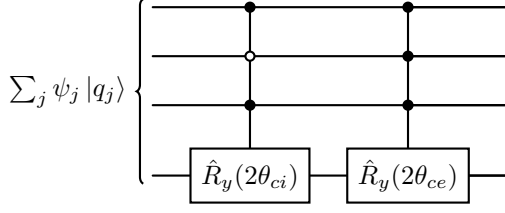


FIG. 4. Quantum circuit implementation of the $\hat{V}_{ce}\hat{V}_{ci}$ product operator in the $\{|q_j\rangle\}$ coin register. The spatial dependence has been suppressed for simplicity.

gates. Therefore, taking into consideration the respective sequences in Eqs.(29),(30) the overall implementation scaling into elementary quantum gates is $O[16(n_{px}^2 + n_{py}^2 + 32)]$. As a result, the qubit lattice algorithm simulates the kinetic part $-c\hat{P}_{E,H} \otimes \hat{\gamma}_{em} \cdot \hat{\mathbf{p}}$ in the plasma-Dirac representation Eq.(9), which reflects the Maxwell equations in the vacuum [18], within a number of elementary quantum gates (by dropping constant factors) $O(n_{px}^2, n_{py}^2)$. This gate complexity is similar by solving the respective free-part of the quantum Dirac or Maxwell equations using Quantum Fourier Transform (QFT).

The unitary potential operators associated with the cyclotron terms $\hat{V}_{ce,i}$ in Eqs.(37) and (38) are two-level \hat{R}_y unitary matrices acting only locally in \mathcal{H}_C and admit an overall implementation as illustrated in Fig.4. Based on this implementation, the decomposition of the product operator $\hat{V}_{ce}\hat{V}_{ci}$ into elementary quantum gates scales as $O(2 \cdot 4^2)$.

Finally, each of the plasma density potential operators in Eqs.(39),(40) is a product of three two-level \hat{R}_y rotations, resulting to a total implementation scaling of $O(6 \cdot 4^2)$ in the $\{|q_j\rangle\}$ register, according to the respective quantum circuits in Figs.5 and 6.

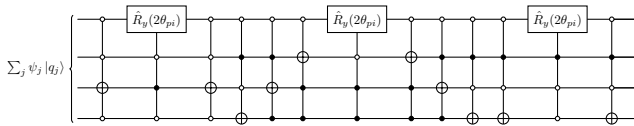


FIG. 5. Quantum circuit implementation of the \hat{V}_{pi} operator in the $\{|q_j\rangle\}$ coin register. The spatial dependence has been suppressed for simplicity.

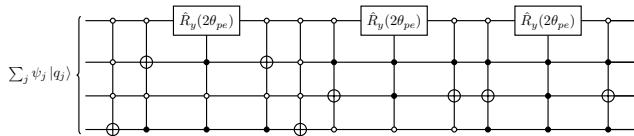


FIG. 6. Quantum circuit implementation of the \hat{V}_{pe} operator in the $\{|q_j\rangle\}$ coin register. The spatial dependence has been suppressed for simplicity.

However, the action of the plasma density potential operators \hat{V}_p 's also depends on the $\{|p\rangle\}$ register according to Eq.(41). Therefore, the overall implementation scaling of the plasma density potential operators in the $\mathcal{H}_C \otimes \mathcal{H}_S$ space accounts for $O(6 \cdot 4^2 \cdot 2^{n_p})$ elementary gates.

From the given construction, our algorithm is explicit without oracle operations and implicit operations and therefore can be implemented on actual quantum hardware.

C. Complexity analysis and comparison with FDTD

Following the discussion in Sec.III B, the overall gate cost $\mathcal{N}_{gate}^q(N)$ (number of elementary gates for quantum algorithm implementation) with N being the number of lattice nodes for a time advancement $t \rightarrow t + \Delta t$ is $\mathcal{N}_{gate}^q(N) = N$. However, for physically relevant applications in electromagnetic scattering in magnetized plasmas from turbulent structures, the density profile of those is considered as a localized inhomogeneity imbued in the uniform background plasma density in the form of filaments or blobs [41, 42]. Therefore, in such scenario the potential operators \hat{V}_p describing a localized inhomogeneity act,

$$\hat{V}_p |\psi(t)\rangle = \sum_{j=0}^{11} \sum_{p=0}^{poly(n_p)} \psi_{j,p} \hat{R}_y(2\theta_p(p)) |q_j\rangle \otimes |p\rangle, \quad (43)$$

with $\theta_p(p) \sim \delta^2 \omega_p(p)$. Then, the respective gate cost is now $\mathcal{N}_{gate}^q(N) = poly(\log(N))$. In the homogeneous case, the only cost-significant gate is effectively the streaming operator, reducing the scaling to $O(\log^2 N)$.

In comparison, the Finite Difference Time Domain (FDTD) algorithms that have been established as prominent tools in the computational studies of electromagnetic wave propagation and scattering [30–33] in complex media, use a staggered lattice in which evaluation of the electromagnetic quantities \mathbf{E}, \mathbf{H} in each lattice cite requires an additional interpolation in each lattice point for anisotropic and inhomogeneous media such as plasmas [33]. As a result, the classical number of gates in the FDTD method for the same time advancement and number of lattice points is $\mathcal{N}_{gate}^c(N) = poly(N)$.

Following [43], a measure for quantum advantage of the proposed quantum algorithm compared to the classical FDTD method is,

$$S_1(N) = \lim_{N \rightarrow \infty} \frac{\mathcal{N}_{gate}^c(N)}{\mathcal{N}_{gate}^q(N)}. \quad (44)$$

Thus, the quantum algorithm exhibits an exponential quantum advantage compared to the FDTD method for localized inhomogeneities. The later speed-up reduces to polynomial for the general case of a global inhomogeneity profile reflecting fluctuations in a uniform background plasma density.

Another measure to establish the quantum advantage is by considering the overall gate complexity for the total simulation time $T = N_t \Delta t$ in respect the desired accuracy ε . Then, the number of gates for simulation time $t \rightarrow t + T$ is $N_t \mathcal{N}_{gate}^{q,c}(N)$. The proposed quantum algorithm operates under a second order scheme, $\Delta t \sim \delta^2$ whereas the Courant–Friedrichs–Lewy (CFL) condition in FDTD connects the spatial resolution linearly with the time, $\Delta t \sim \delta$. Consequently, for the 2D case, $N_t = O(N)$ for the QLA and $N_t = O(\sqrt{N})$ for the FDTD. Therefore, the gate complexities for the total simulation time \mathcal{N}_{gate}^T read,

$$\begin{aligned} \mathcal{N}_{gate}^{q,T}(N) &= N^2, \quad (\text{general case}), \\ \mathcal{N}_{gate}^{q,T}(N) &= N \text{poly}(\log N), \quad (\text{localized inhomogeneity}), \\ \mathcal{N}_{gate}^{c,T}(N) &= \sqrt{N} \text{poly}(N), \quad (\text{FDTD}). \end{aligned} \quad (45)$$

Equivalently, the gate complexities in Eq.(45) in terms of the desired accuracy ε read,

$$\begin{aligned} \mathcal{N}_{gate}^{q,T}(\varepsilon) &= T^4/\varepsilon^2, \quad (\text{general case}), \\ \mathcal{N}_{gate}^{q,T}(\varepsilon) &= (T^2/\varepsilon) \text{poly}\left(\log \frac{T^2}{\varepsilon}\right), \quad (\text{localized inhomogeneity}), \\ \mathcal{N}_{gate}^{c,T}(\varepsilon) &= (T^4/\varepsilon)^{1/3} \text{poly}\left(\frac{T^{8/3}}{\varepsilon^{2/3}}\right), \quad (\text{FDTD}). \end{aligned} \quad (46)$$

The comparison between the respective ranges of gate complexities for the QLA and FDTD for $\kappa = 1, 2$ and 3 dimensions, is presented in the Table I.

Therefore, using Eq.(46) and Table I to evaluate the complexity comparison criterion [43],

$$S_2(\varepsilon) = \lim_{\varepsilon \rightarrow 0} \frac{\mathcal{N}_{gate}^{c,T}(\varepsilon)}{\mathcal{N}_{gate}^{q,T}(\varepsilon)}, \quad (47)$$

we obtain a strong polynomial quantum speedup of the quantum algorithm compared to the FDTD for $\kappa \geq 2$ and an exponential strong quantum speed up for the scattering off localized plasma inhomogeneities.

Consequently, the proposed qubit lattice algorithm not only possesses an explicit implementation structure but also exhibits, at worst case, polynomial advantage compared to the FDTD method for full-wave simulation of Maxwell simulations in cold inhomogeneous and magnetized plasmas.

IV. GENERALIZING TO THE DISSIPATIVE CASE

A. The dissipative model

Introducing the simplest form of dissipation requires the existence of a phenomenological collision frequency ν between the two species (ions-electrons) in plasma.

Then, the frequency dependent Stix permittivity matrix $\tilde{\epsilon}_\nu(\omega)$ is [34, 36],

$$\tilde{\epsilon}_\nu(\omega) = \begin{bmatrix} S_\nu & -iD_\nu & 0 \\ iD_\nu & S_\nu & 0 \\ 0 & 0 & P_\nu \end{bmatrix} \quad (48)$$

with

$$\begin{aligned} S_\nu &= \epsilon_0 \left(1 - \sum_{j=i,e} \frac{\omega_{pj}^2 (\omega + i\nu)}{\omega (\omega + i\nu) - \omega_{cj}^2} \right) \\ D_\nu &= \epsilon_0 \sum_{j=i,e} \frac{\omega_{cj} \omega_{pj}^2}{\omega [(\omega + i\nu)^2 - \omega_{cj}^2]} \\ P_\nu &= \epsilon_0 \left(1 - \sum_{j=i,e} \frac{\omega_{pj}^2}{\omega (\omega + i\nu)} \right). \end{aligned} \quad (49)$$

Obviously, now $\tilde{\epsilon}_\nu(\omega) \neq \tilde{\epsilon}_\nu^\dagger(\omega)$ since there is energy dissipation. For $\nu = 0$ we recover the Hermitian (energy-preserving) counterpart $\tilde{\epsilon}(\omega)$ in Eqs.(5),(6).

In contrast with the conservative case in Eq.(11), the susceptibility kernel $\hat{K}_\nu u(\mathbf{r}, t)$ is characterized by both memory and dissipative effects,

$$\hat{K}_\nu(t) = \epsilon_0 \sum_{j=i,e} \begin{bmatrix} K_\nu^{(xx)} & K_\nu^{(xy)} & 0 \\ -K_\nu^{(xy)} & K_\nu^{(yy)} & 0 \\ 0 & 0 & K_\nu^{(zz)} \end{bmatrix}, \quad (50)$$

with

$$\begin{aligned} K_\nu^{(xx)} &= K_\nu^{(yy)} = \frac{\omega_{pj}^2}{\omega_{cj}^2 + \nu^2} \left(e^{-\nu t} (\omega_{cj} \sin \omega_{cj} t - \nu \cos \omega_{cj} t) - \nu \right) \\ K_\nu^{(xy)} &= \frac{\omega_{pj}^2}{\omega_{cj}^2 + \nu^2} \left(e^{-\nu t} (\omega_{cj} \cos \omega_{cj} t + \nu \sin \omega_{cj} t) + \omega_{cj} \right) \\ K_\nu^{(zz)} &= \frac{\omega_{pj}^2}{\nu} (1 - e^{-\nu t}). \end{aligned} \quad (51)$$

The total conductivity current is now,

$$\mathbf{J}_{\nu,c} = \int_0^t \frac{\partial \hat{K}_\nu(\mathbf{r}, t - \tau)}{\partial t} \mathbf{u}(\mathbf{r}, \tau) d\tau, \quad (52)$$

with

$$\frac{\partial \hat{K}_\nu}{\partial t} = e^{-\nu t} \frac{\partial \hat{K}}{\partial t}. \quad (53)$$

The $\partial \hat{K}_\nu / \partial t$ term in Eq.(53) is the conservative counterpart, provided in [21]. Based on the relation (53) and following the same procedure as in [21] the resulted dissipative plasma-Dirac equation,

$$i \frac{\partial \psi_\nu}{\partial t} = \left[-c \hat{P}_{E,B} \otimes \hat{\gamma}_{em} \cdot \hat{\mathbf{p}} + \hat{V}_\nu(\mathbf{r}) \right] \psi_\nu, \quad (54)$$

TABLE I. Gate scalings for the quantum QLA versus the classical FDTD methods. The dimensionality of the problem is given by the parameter $\kappa = 1, 2, 3$.

Method	$\mathcal{N}_{gate}(N)$	$\mathcal{N}_{gate}^T(N)$	$\mathcal{N}_{gate}^T(\varepsilon)$
FDTD	$O[\text{poly}(N)]$	$O[N^{1/\kappa} \text{poly}(N)]$	$O[(T^2/\varepsilon) \text{poly}(T^2/\varepsilon)^\kappa]$
QLA	$O(\log^2 N) - O(N)$	$O(N^{2/\kappa} \log^2 N) - O(N^{\frac{2+\kappa}{\kappa}})$	$O[(T^2/\varepsilon) \log^2(T^2/\varepsilon)^{\kappa/2}] - O[(T^2/\varepsilon)^{\frac{2+\kappa}{2}}]$

now has the potential term $\hat{V}_\nu(\mathbf{r})$ with an anti-Hermitian diagonal component,

$$\hat{V}_\nu(\mathbf{r}) = \begin{bmatrix} 0_{3 \times 3} & 0_{3 \times 3} & -i\omega_{pi} & -i\omega_{pe} \\ 0_{3 \times 3} & 0_{3 \times 3} & 0_{3 \times 3} & 0_{3 \times 3} \\ i\omega_{pi} & 0_{3 \times 3} & \omega_{ci}\hat{S}_z - i\nu & 0_{3 \times 3} \\ i\omega_{pe} & 0_{3 \times 3} & 0_{3 \times 3} & \omega_{ce}\hat{S}_z - i\nu \end{bmatrix}. \quad (55)$$

In terms of the conservative generator of dynamics $\hat{D} = -c\hat{P}_{E,B} \otimes \hat{\gamma}_{em} \cdot \hat{\mathbf{p}} + \hat{V}(\mathbf{r})$, Eq.(55) reads,

$$i\frac{\partial \psi_\nu}{\partial t} = (\hat{D} - i\hat{D}_{diss})\psi_\nu, \quad -i\hat{D}_{diss} = \hat{V}_\nu - \hat{V}. \quad (56)$$

The \hat{D}_{diss} operator in Eq.(56) is a diagonal Hermitian and positive definite matrix so for the $-i\hat{D}_{diss}$ to generate pure collisional dissipation.

B. Post-selective time marching implementation procedure

Treating the collisional plasma Dirac equation (56) in the context of unitary quantum computing can be accomplished through two distinct implementation roots which share a post-selective nature.

The first path consists of using a directly a first order Trotter product formula by separating the unitary from the non-unitary part. Then, according to Eq.(56) the Trotterized evolution reads

$$|\psi_\nu(t + \Delta t)\rangle = e^{-i\Delta t \hat{D}} e^{-\Delta t \hat{D}_{diss}} |\psi_\nu(t)\rangle + O(\Delta t^2). \quad (57)$$

The exponential non-unitary part in the Trotterized evolution Eq.(57) can be easily evaluated as

$$\hat{K} = e^{-\Delta t \hat{D}_{diss}} = \text{diag}(I_{6N \times 6N}, e^{-\nu \Delta t} I_{6N \times 6N}). \quad (58)$$

Because we have established pure dissipation, the respective non-trivial diagonal elements of \hat{K} matrix is can be written as $e^{-\nu \Delta t} = \cos(\phi/2)$. As a result, we can decompose the non-unitary diagonal operator \hat{K} in two unitary diagonal components,

$$\hat{K} = \frac{\hat{K}_z + \hat{K}_z^\dagger}{2}, \quad (59)$$

with

$$\hat{K}_z = \begin{bmatrix} I_{6N \times 6N} & 0 \\ 0 & e^{-i\phi/2} I_{6N \times 6N} \end{bmatrix}. \quad (60)$$

Based on the unitary sum decomposition of the the non-unitary matrix \hat{K} in Eq.(59), its implementation follows the Linear Combination of Unitaries (LCU) method [44] with the introduction of one ancillary qubit as follows. First we define the following unitary operators,

$$\hat{U}_{prep} : |0\rangle \rightarrow \frac{1}{\sqrt{2}}(|0\rangle + |1\rangle), \quad (61)$$

$$\hat{U}_{select} = |0\rangle\langle 0| \otimes \hat{K}_z + |1\rangle\langle 1| \otimes \hat{K}_z^\dagger, \quad (62)$$

where $\hat{U}_{prep} = \hat{H}$ is the Hadamard gate. The explicit form of the \hat{U}_{select} operator,

$$\hat{U}_{select} = \begin{bmatrix} \hat{K}_z & 0 \\ 0 & \hat{K}_z^\dagger \end{bmatrix}, \quad (63)$$

dictates that it is a diagonal unitary operator composed of $6N$ two-level $\hat{R}_z(\phi)$ gates and can be implemented within $O[\text{poly}(n_p)]$ [45]. In case we had different and inhomogeneous dissipation rates, then the implementation scaling would significantly increases to $O(2^{n_p+1})$ [46].

Then, by applying with the unitary operator

$$\hat{U} = (\hat{H} \otimes I_{12N \times 12N}) \hat{U}_{select} (\hat{H} \otimes I_{12N \times 12N}). \quad (64)$$

into the composite state $|0\rangle \otimes |\psi(t)\rangle$, we can probabilistically implement the non-unitary \hat{K} matrix,

$$\hat{U}(|0\rangle \otimes |\psi_\nu(t)\rangle) = |0\rangle \hat{K} |\psi_\nu(t)\rangle + \frac{1}{2} |1\rangle (\hat{K}_z - \hat{K}_z^\dagger) |\psi_\nu(t)\rangle. \quad (65)$$

A unitary controlled operation in respect to the 0-bit for the unitary part $e^{-i\Delta t \hat{D}}$, followed by a measurement in the output state in Eq.(65) with respect to $|0\rangle$ state produces the non-unitary Trotterized evolution in Eq.(57). The respective quantum circuit implementation for the Trotterized time advancement $t \rightarrow t + \Delta t$ is depicted in Fig.7.

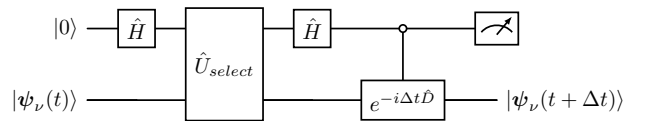


FIG. 7. Quantum circuit implementation of the non-unitary Trotterized evolution in Eq.(57). The implementation technique and scaling for the unitary operator $e^{-i\Delta t \hat{D}}$ has been detailed in Sec.II.

On a final note, the LCU dilation operation $\hat{\mathcal{U}}$ is a diagonalization of the one-qubit Sz.-Nagy dilation technique for the non unitary \hat{K} operator [22, 47],

$$\hat{\mathcal{U}}_K^{SN} = \begin{bmatrix} \hat{K} & -\sqrt{I_{12N \times 12N} - \hat{K}^2} \\ \sqrt{I_{12N \times 12N} - \hat{K}^2} & \hat{K} \end{bmatrix}. \quad (66)$$

The Sz.-Nagy dilation matrix (66) acts as a guaranteed block encoding of the non-unitary operator \hat{K} .

Let us now delve into the post-selective nature for a total simulation time of $T = N_t \Delta t$. For the infinitesimal time advancement $t \rightarrow t + \Delta t$ the success probability of the post selection is,

$$p_{success}(\Delta t) = \langle \psi(t) | \hat{K}^2 | \psi(t) \rangle. \quad (67)$$

$$p_{success}(T) = \|\psi_\nu(t + \Delta t)\|^2 \cdot \frac{\|\psi_\nu(t + 2\Delta t)\|^2}{\|\psi_\nu(t + \Delta t)\|^2} \dots \frac{\|\psi_\nu(t + (N_t - 1)\Delta t)\|^2}{\|\psi_\nu(t + (N_t - 2)\Delta t)\|^2} \cdot \frac{\|\psi_\nu(t + T)\|^2}{\|\psi_\nu(t + (N_t - 1)\Delta t)\|^2} = \|\psi_\nu(t + T)\|^2. \quad (69)$$

In Appendix A, it is demonstrated that the total success probability in Eq.(69) of the proposed post-selective algorithm is non-vanishing, $p_{success}(T) \geq 1/e$, in the limit $N_t \rightarrow \infty$. The latter has been firstly investigated by considering different time-scales and dissipation strengths in [22] for simulating Maxwell equations in dissipative media and computationally demonstrated for simulating the advection-diffusion equation [49].

Consequently, the number of the required copies for obtaining the overall non-unitary evolution from the normalized initial state $|\psi_\nu(t)\rangle$ to the final normalized state is $1/p_{success}(T) \sim e$. Thus, the proposed post-selective scheme not only allows for an efficient implementation without requiring many copies of the initial state with parallel evolution but also avoids the need for amplitude amplification [50] in the output state for a non-vanishing measurement. As a result, the quantum advantage established in the conservative case is retained in this post-selective protocol, as the implementation overhead scales at most by a multiplicative factor of $2e$.

Another implementation path would be the "QLAza" of the dissipative equation (55) resulting to a implementation sequence, similar with that of Eq.(24),

$$|\psi(t + \Delta t)\rangle = \hat{V}_{pe} \hat{V}_{pi} \hat{V}_{\nu,ce} \hat{V}_{\nu,ci} \hat{\mathcal{U}}_{QLA} |\psi(t)\rangle, \quad (70)$$

where the operators $\hat{V}_{\nu,ce}, \hat{V}_{\nu,ci}$ are now non-unitary. Notice that since the dissipation is introduced through a diagonal form it is expected that only the $\hat{V}_{ce}, \hat{V}_{ci}$ matrices will be affected. Once again, decomposing the non-unitary operators into a sum of unitary matrices enables the implementation using the LCU method.

Expanding the \hat{K} operator to first order in $\nu \Delta t$, Eq.(67) reads,

$$p_{success}(\Delta t) \approx 1 - 2\nu \Delta t \sum_{j=6}^{11} \sum_p |\psi_{\nu,j,p}(t)|^2. \quad (68)$$

In general, for $p_{success}(\Delta t) \sim O(1)$ the Trotter time-step has to be selected as $\Delta t \ll 1/2\nu$. The overall success probability $p_{success}(T)$, for implementing the normalized non-unitary evolution $|\psi_\nu(t)\rangle \rightarrow |\psi_\nu(t + T)\rangle / \|\psi_\nu(t + T)\|$ with $|\psi_\nu(t + T)\rangle = (e^{-i\Delta t \hat{D}} e^{-\Delta t \hat{D}_{diss}})^{N_t} |\psi_\nu(t)\rangle$ to an error ε [48] after N_t repetitions of the quantum circuit in Fig.7 with intermediate post-selections is,

V. CONCLUSIONS

Electromagnetic waves are ubiquitous in nature, playing a pivotal role in a wide range of real-world applications. In this paper, we explore the potential impact of quantum computing on the study of electromagnetic wave propagation and scattering in complex media by proposing a quantum algorithm to simulate Maxwell equations in magnetized plasmas. The scope of this paper aligns with efforts to leverage quantum computing as a powerful alternative to classical simulations in plasma physics and fusion research [21, 51–53].

The main contributions of the paper are threefold. Firstly, the proposed qubit lattice algorithm for the energy-conserving case, features an explicit implementation structure suitable for testing on contemporary quantum hardware. More importantly, we have established a theoretical quantum speed-up over the widely used classical FDTD method for scattering studies in fusion plasmas. Finally, we develop a post-selective implementation procedure for non-unitary evolution in the presence of dissipation, modeled through a simple collisional mechanism, with an optimal, non-vanishing overall success probability. In that way, the number of the required copies for the proposed probabilistic quantum implementation to be successful is of order $O(1)$. Consequently, the resource overhead remains a multiplicative factor of the conservative case, preserving the quantum advantage.

Our findings suggest that quantum computing has the potential to revolutionize the computational study of electromagnetic wave propagation and scattering in complex media. In the near future we will pursue an actual implementation in quantum hardware to benchmark the theoretical performance of the quantum algorithm.

ACKNOWLEDGMENTS

This work has been carried out within the framework of the EUROfusion Consortium, funded by the European Union via the Euratom Research and Training Programme (Grant Agreement No 101052200 — EUROfusion). Views and opinions expressed are however those of the authors only and do not necessarily reflect those of the European Union or the European Commission. Neither the European Union nor the European Commission can be held responsible for them. E.K., K.H, and C.T., acknowledge valuable discussions with Ó. Amaro, L.I.I. Gamiz, A. Papadopoulos, I. Theodonis, Y. Kominis, P. Papagiannis and G. Fikioris. A.K.R., G.V., M.S. and L.V. are supported by the US Department of Energy under Grant Nos. DE-SC0021647, DE-FG02-91ER-54109, DE-SC0021651, DE-SC0021857 and DE-SC0021653.

Appendix A: Non-vanishing implementation probability

By defining the normalized states,

$$|\phi(t + k\Delta t)\rangle = \frac{|\psi_\nu(t + k\Delta t)\rangle}{\|\psi_\nu(t + k\Delta t)\|}, \quad k = 0, 1, \dots, N_t, \quad (\text{A1})$$

with $|\phi(t)\rangle = |\psi_\nu(t)\rangle$, $\|\psi_\nu(t)\| = 1$, the total success probability in Eq.(69) reads,

$$p_{\text{success}}(T) = \prod_{k=0}^{N_t-1} \langle \phi(t + k\Delta t) | \hat{K}^\dagger \hat{K} | \phi(t + k\Delta t) \rangle. \quad (\text{A2})$$

Substituting Eq.(58) for the diagonal and non-unitary operator \hat{K} into Eq.(A2) and taking advantage that normalization of the $|\phi\rangle$ states, we obtain

$$p_{\text{success}}(T) = \prod_{k=0}^{N_t-1} \left[1 - (1 - e^{-\beta}) \sum_{j=6}^{11} \sum_p |\phi_{j,p}(t + k\Delta t)|^2 \right], \quad (\text{A3})$$

with $\beta = 2\nu\Delta t$. Setting,

$$a_k = \sum_{j=6}^{11} \sum_p |\phi_{j,p}(t + k\Delta t)|^2, \quad 0 \leq a_k < 1, \quad (\text{A4})$$

the Eq.(A3) in the limit $N_t \rightarrow \infty$ is compactly written as an infinite product of the form,

$$\lim_{N_t \rightarrow \infty} p_{\text{success}}(T) = \prod_{k=0}^{\infty} \left[1 - (1 - e^{-\beta}) a_k \right] \quad (\text{A5})$$

The infinite product in Eq.(A5) converges to a non-zero positive number if and only if the following infinite sum converges [54],

$$\sum_{k=0}^{\infty} a_k < \infty. \quad (\text{A6})$$

Notice that in our case the a_k in Eq.(A4) includes terms associated with the dissipative subspace defined by the \hat{K} operator. In addition, the dissipation mechanism dictated by the form of \hat{K} proposes that $a_k = a_{k-1}e^{-\beta}$. Thus,

$$a_k = a_0 e^{-k\beta}. \quad (\text{A7})$$

For more complex dissipative processes, instead of an exponential decay, a polynomial decay could be present $a_k = a_0 k^{-x}$. However, the infinite sum in Eq.(A6) converges, and therefore the probability is non-vanishing, only when $x > 1$.

In the $\beta \ll 1$ limit (recall Eq.(68)) together with Eq.(A7), the infinite product in Eq.(A5) takes the simple form,

$$P = \lim_{N_t \rightarrow \infty} p_{\text{success}}(T) = \prod_{k=0}^{\infty} (1 - \beta a_0 e^{-k\beta}) \quad (\text{A8})$$

Taking the $\ln P$ and the approximation $\beta \ll 1$ we obtain,

$$\ln P = \sum_{k=0}^{\infty} \ln(1 - \beta a_0 e^{-k\beta}) \approx \beta a_0 \sum_{k=0}^{\infty} e^{-k\beta} \quad (\text{A9})$$

The infinite sum in Eq.(A9) is the limit of geometric series

$$\sum_{k=0}^{\infty} e^{-k\beta} = \frac{1}{1 - e^{-\beta}} \approx \frac{1}{\beta}, \quad \beta \ll 1. \quad (\text{A10})$$

Finally,

$$\lim_{N_t \rightarrow \infty} p_{\text{success}}(T) = e^{\ln P} = e^{-a_0} \geq \frac{1}{e}, \quad (\text{A11})$$

since $0 \leq a_0 < 1$.

-
- [1] Y. Aharonov, L. Davidovich, and N. Zagury, Quantum random walks, *Phys. Rev. A* **48**, 1687 (1993).
 [2] A. Ambainis, E. Bach, A. Nayak, A. Vishwanath, and

J. Watrous, One-dimensional quantum walks, in *Proceedings of the Thirty-Third Annual ACM Symposium on Theory of Computing*, STOC '01 (Association for Com-

- puting Machinery, New York, NY, USA, 2001) p. 37–49.
- [3] A. M. Childs, R. Cleve, E. Deotto, E. Farhi, S. Gutmann, and D. A. Spielman, Exponential algorithmic speedup by a quantum walk, in *Proceedings of the Thirty-Fifth Annual ACM Symposium on Theory of Computing*, STOC '03 (Association for Computing Machinery, New York, NY, USA, 2003) p. 59–68.
 - [4] A. M. Childs, On the relationship between continuous- and discrete-time quantum walk, *Commun. Math. Phys.* **294**, 581 (2010).
 - [5] D. W. Berry and A. M. Childs, Black-box Hamiltonian simulation and unitary implementation, *Quant. Inf. Comput.* **12**, 0029 (2012).
 - [6] D. W. Berry, A. M. Childs, and R. Kothari, Hamiltonian simulation with nearly optimal dependence on all parameters, in *Proceedings of the 2015 IEEE 56th Annual Symposium on Foundations of Computer Science (FOCS)*, FOCS '15 (2015) p. 792–809.
 - [7] A. M. Childs, Universal computation by quantum walk, *Phys. Rev. Lett.* **102**, 180501 (2009).
 - [8] F. m. c. Fillion-Gourdeau, S. MacLean, and R. Laflamme, Algorithm for the solution of the dirac equation on digital quantum computers, *Phys. Rev. A* **95**, 042343 (2017).
 - [9] L. Mlodinow and T. A. Brun, Discrete spacetime, quantum walks, and relativistic wave equations, *Phys. Rev. A* **97**, 042131 (2018).
 - [10] U. Nzongani, N. Eon, I. Márquez-Martín, A. Pérez, G. Di Molfetta, and P. Arrighi, Dirac quantum walk on tetrahedra, *Phys. Rev. A* **110**, 042418 (2024).
 - [11] I. Białynicki-Birula, Weyl, dirac, and maxwell equations on a lattice as unitary cellular automata, *Phys. Rev. D* **49**, 6920 (1994).
 - [12] B. M. Boghosian and W. Taylor, Quantum lattice-gas model for the many-particle schrödinger equation in d dimensions, *Phys. Rev. E* **57**, 54 (1998).
 - [13] J. Yepez and B. Boghosian, An efficient and accurate quantum lattice-gas model for the many-body schrödinger wave equation, *Computer Physics Communications* **146**, 280 (2002).
 - [14] S. Succi, F. Fillion-Gourdeau, and S. Palpacelli, Dirac quantum walk on tetrahedra, *EPJ Quantum Technol.* **02**, 042418 (2015).
 - [15] J. Yepez, An efficient and accurate quantum algorithm for the dirac equation (2002), [arXiv:quant-ph/0210093 \[quant-ph\]](https://arxiv.org/abs/quant-ph/0210093).
 - [16] G. Vahala, E. Koukoutsis, M. Soe, K. Hizanidis, L. Vahala, and A. K. Ram, Qubit lattice algorithms, *Radiat. Eff. Defects Solids* **178**, 1350 (2023).
 - [17] G. Vahala, L. Vahala, M. Soe, and A. K. Ram, Unitary quantum lattice simulations for maxwell equations in vacuum and in dielectric media, *J. Plasma Phys.* **86**, 905860518 (2020).
 - [18] E. Koukoutsis, K. Hizanidis, A. K. Ram, and G. Vahala, Dyson maps and unitary evolution for maxwell equations in tensor dielectric media, *Phys. Rev. A* **107**, 042215 (2023).
 - [19] G. Vahala, M. Soe, L. Vahala, A. K. Ram, E. Koukoutsis, and K. Hizanidis, Qubit lattice algorithm simulations of maxwell's equations for scattering from anisotropic dielectric objects, *Comput. Fluids* **266**, 106039 (2023).
 - [20] G. Vahala, M. Soe, E. Koukoutsis, K. Hizanidis, L. Vahala, and A. K. Ram, Qubit lattice algorithms based on the schrödinger-dirac representation of maxwell equations and their extensions, in *Schrödinger Equation*, edited by M. B. Tahir, M. Sagir, M. I. Khan, and M. Rafique (IntechOpen, Rijeka, 2023) Chap. 7.
 - [21] E. Koukoutsis, K. Hizanidis, G. Vahala, M. Soe, L. Vahala, and A. K. Ram, Quantum computing perspective for electromagnetic wave propagation in cold magnetized plasmas, *Phys. Plasmas* **30**, 122108 (2023).
 - [22] E. Koukoutsis, K. Hizanidis, A. K. Ram, and G. Vahala, Quantum simulation of dissipation for maxwell equations in dispersive media, *Future Gener. Comput. Syst.* **159**, 221 (2024).
 - [23] S. Sinha and P. Russer, Quantum computing algorithm for electromagnetic field simulation, *Quantum Inf. Process.* **09**, 385 (2010).
 - [24] P. C. S. Costa, S. Jordan, and A. Ostrander, Quantum algorithm for simulating the wave equation, *Phys. Rev. A* **99**, 012323 (2019).
 - [25] J. Zhang, F. Feng, and Q. J. Zhang, Quantum method for finite element simulation of electromagnetic problems, in *2021 IEEE MTT-S International Microwave Symposium (IMS)* (2021) pp. 120–123.
 - [26] R. Novak, Quantum algorithms in electromagnetic propagation modelling for telecommunications, *IEEE Access* **11**, 111545 (2023).
 - [27] I. Novikau, I. Dodin, and E. Startsev, Simulation of linear non-hermitian boundary-value problems with quantum singular-value transformation, *Phys. Rev. Appl.* **19**, 054012 (2023).
 - [28] Jin, Shi, Liu, Nana, and Ma, Chuwen, Quantum simulation of maxwell's equations via schrödingerisation, *ESAIM: M2AN* **58**, 1853 (2024).
 - [29] N. Nguyen and R. Thompson, Solving maxwells equations using variational quantum imaginary time evolution (2024), [arXiv:2402.14156 \[quant-ph\]](https://arxiv.org/abs/2402.14156).
 - [30] K. Yee, Numerical solution of initial boundary value problems involving maxwell's equations in isotropic media, *IEEE Trans. Antennas Propag.* **14**, 302 (1966).
 - [31] J. Schneider and S. Hudson, A finite-difference time-domain method applied to anisotropic material, *IEEE Trans. Antennas Propag.* **41**, 994 (1993).
 - [32] J. H. Lee and D. Kalluri, Three-dimensional fdtd simulation of electromagnetic wave transformation in a dynamic inhomogeneous magnetized plasma, *IEEE Trans. Antennas and Propag.* **47**, 1146 (1999).
 - [33] C. Tsironis and A. Papadopoulos, Parallelization of a 3d fdtd code and physics studies of electromagnetic wave propagation in fusion plasmas, *J. Electromagn. Waves Appl.* **37**, 1366 (2023).
 - [34] H. T. Stix, *Waves in Plasmas* (American Institute of Physics, 1992).
 - [35] A. Mostafazadeh, Pseudo-hermiticity versus pt-symmetry. ii. a complete characterization of non-hermitian hamiltonians with a real spectrum, *J. Math. Phys.* **43**, 2814 (2002).
 - [36] A. Bers, *Plasma Physics and Fusion Plasma Electrodynamics* (Oxford University Press, 2016).
 - [37] N. Bao and G. Suer, Exploiting recursive structures for the design of novel quantum primitives (2024), [arXiv:2410.13927 \[quant-ph\]](https://arxiv.org/abs/2410.13927).
 - [38] A. Barenco, C. H. Bennett, R. Cleve, D. P. DiVincenzo, N. Margolus, P. Shor, T. Sleator, J. A. Smolin, and H. Weinfurter, Elementary gates for quantum computation, *Phys. Rev. A* **52**, 3457 (1995).
 - [39] A. Acin, A. Andrianov, E. Jane, and R. Tarrach, Three-qubit pure-state canonical forms, *J. Phys. A: Math. Gen.*

- 34**, 6725 (2001).
- [40] U. Nzongani, J. Zylberman, C.-E. Doncechi, A. Pérez, F. Debbasch, and P. Arnault, Quantum circuits for discrete-time quantum walks with position-dependent coin operator, *Quantum Inf. Process* **22**, 270 (2023).
- [41] A. K. Ram, K. Hizanidis, and Y. Kominis, Scattering of radio frequency waves by blobs in tokamak plasmas, *Phys. Plasmas* **20**, 056110 (2013).
- [42] A. K. Ram and K. Hizanidis, Scattering of radio frequency waves by cylindrical density filaments in tokamak plasmas, *Phys. Plasmas* **23**, 022504 (2016).
- [43] A. Papageorgiou and J. F. Traub, Measures of quantum computing speedup, *Phys. Rev. A* **88**, 022316 (2013).
- [44] A. M. Childs and N. Wiebe, Hamiltonian simulation using linear combinations of unitary operations, *Quantum Info. Comput.* **12**, 901–924 (2012).
- [45] T. Hogg, C. Mochon, W. Polak, and E. Rieffel, Tools for quantum algorithms, *Int. J. Mod. Phys. C* **10**, 1347 (1999).
- [46] S. S. Bullock and I. L. Markov, Asymptotically optimal circuits for arbitrary n-qubit diagonal comutations, *Quantum Inf. Comput.* **4**, 27–47 (2004).
- [47] A. W. Schlimgen, K. Head-Marsden, L. M. Sager-Smith, P. Narang, and D. A. Mazziotti, Quantum state preparation and nonunitary evolution with diagonal operators, *Phys. Rev. A* **106**, 022414 (2022).
- [48] A. M. Childs, Y. Su, M. C. Tran, N. Wiebe, and S. Zhu, Theory of Trotter Error with Commutator Scaling, *Phys. Rev. X* **11**, 011020 (2021).
- [49] P. Over, S. Bengoechea, P. Brearley, S. Laizet, and T. Rung, *Quantum algorithm for the advection-diffusion equation with optimal success probability* (2024), arXiv:2410.07909 [quant-ph].
- [50] G. Brassard, P. Høyer, M. Mosca, and A. Tapp, Quantum amplitude amplification and estimation (American Mathematical Society, 2002) p. 53–74.
- [51] I. Y. Dodin and E. A. Startsev, On applications of quantum computing to plasma simulations, *Physics of Plasmas* **28**, 092101 (2021).
- [52] Ó. Amaro and D. Cruz, *A living review of quantum computing for plasma physics* (2023), arXiv:2302.00001 [physics.plasm-ph].
- [53] I. Joseph, Y. Shi, M. D. Porter, A. R. Castelli, V. I. Geyko, F. R. Graziani, S. B. Libby, and J. L. DuBois, Quantum computing for fusion energy science applications, *Phys. Plasmas* **30**, 010501 (2023).
- [54] K. Knopp, *Theory and Application of Infinite Series* (Dover Publications, 1990).